Research Article

Zehba Raizah, Anwar Saeed*, Muhammad Bilal, Ahmed M. Galal, and Ebenezer Bonyah

Parametric simulation of stagnation point flow of motile microorganism hybrid nanofluid across a circular cylinder with sinusoidal radius

https://doi.org/10.1515/phys-2022-0205
received April 22, 2022; accepted January 02, 2023

Abstract: The article explores the three-dimensional stream of silver (Ag), magnesium oxide (MgO), and motile microorganism water-based hybrid nanofluids as independent of time through a circular cylinder with a sinusoidal radius. The goal of this research is to optimize the rate of energy and mass transfer through a circular cylinder having a periodic radius. The phenomena are simulated as a system of partial differential equations containing momentum, temperature, concentration, and the profile of motile microbes, which were then simplified to a dimensionless system of ordinal differential equations using the similarity technique. The problem is solved by using the parametric continuation method, which is a numerical methodology. From the analysis, it has been perceived that both the energy and velocity fields significantly enhance with the rising effect of hybrid nanoparticles (Ag–MgO). The effect of chemical reaction enhances the mass transition rate because chemical reaction parameter influence exercises the molecules inside the fluid. The motile microorganism outline is elevated with the increment of Lewis and Peclet number.

*** Corresponding author: Anwar Saeed,** Center of Excellence in Theoretical and Computational Science (TaCS-CoE), Faculty of Science, King Mongkut's University of Technology Thonburi (KMUTT), 126 Pracha Uthit Rd., Bang Mod, Thung Khru, Bangkok, 10140, Thailand, e-mail: anwarsaeed769@gmail.com
Zehba Raizah: Department of Mathematics, College of Science, King Khalid University, Abha, Saudi Arabia
Muhammad Bilal: Sheikh Taimur Academic Block-II, Department of Mathematics, University of Peshawar, 25120, Khyber Pakhtunkhwa, Pakistan
Ahmed M. Galal: Department of Mechanical Engineering, College of Engineering in Wadi Alddawasir, Prince Sattam Bin Abdulaziz University, Wadi Alddawasir, Saudi Arabia; Production Engineering and Mechanical Design Department, Faculty of Engineering, Mansoura University, P.O 35516, Mansoura, Egypt
Ebenezer Bonyah: Department of Mathematics Education, Akenten Appiah Menka University of Skills Training and Entrepreneurial Development, Kumasi, Ghana

Keywords: hybrid nanofluid, motile microorganism, parametric continuation method, circular cylinder, sinusoidal radius

Nomenclature

c	noddle point
u, v, w	velocity component
k_{hnf}	thermal conductivity
D_{hnf}	mass diffusivity
$(\rho C_p)_{hnf}$	volumetric heat capacity
D_n	microorganism diffusion
N	motile microbes' density
Re_b	Reynolds number
Pe	Peclet number
$\Theta(\eta)$	dimensionless energy profile
C_w	concentration over the surface
C_∞	ambient concentration
C_p	heat capacity
$\Phi(\eta)$	dimensionless mass transition
Sc	Schmidth number
$x_e^\star$	streamlines
μ_{hnf}	dynamic viscosity
ρ_{hnf}	density
T	temperature
Pr	Prandtl number
K	chemical reaction
Le	Lewis number
$h(\eta)$	dimensionless motile microorganism
$f'(\eta)$	dimensionless velocity profile
ϕ_1, ϕ_2	volume friction
T_∞	ambient temperature
Nu	Nusselt number
ν	kinematic viscosity of fluid
η	similarity variable
C_f	skin friction

a^*, b^*	stream coefficients
β	constant

1 Introduction

Many engineering operations include flow through a circular cylinder, but far less research has been done on flow over a cylinder in a restricted domain. Several phenomena depend on wall upshots, such as blood flow through medical equipment in veins, flow over cylindrical objects near walls, and so on [1–3]. Moreover, the analysis of fluid flow across or over an irregular surface received enough attention. When regular sinusoidal ridges are present, a three-dimensional (3D) printer, owing to desired vibrations throughout the printing procedure, prompts research of the resultant flow consequences [4]. Salahuddin *et al.* [5] documented the consequence of variously configured nanomaterials on the thermal characteristics and flow efficiency of ferrofluid across rigid and sinusoidal surfaces. Wu *et al.* [6] utilized several active mechanism wind tunnel to evaluate the aerodynamic workloads of a sinusoidal cylinder. Changing the amplitude and frequency produces a succession that is entirely coherent in the streamwise direction. Bilal *et al.* [7] described an extending cylinder-induced incompressible Maxwell nanofluid flow accompanied by an unfluctuating suction/injection effect. It was determined that the impacts of the thermophoresis considerably increased the velocity of mass transference, while the consequences of the viscosity factor's expansion substantially decreased the velocity curve. Seo *et al.* [8] numerically estimated the free convection in a broad, diagonal domain with a sinusoidal cylinder. In order to outperform a circular cylinder in terms of overall heat exchange, the sinusoidal cylinders were investigated. Bilal *et al.* [9] addressed the hybrid nanoliquid's Darcy–Forchhemier mixed convective flow across an angled, expanding cylinder. Alharbi *et al.* [10] documented the magnetic characteristics of nanoliquid flow with energy flux in a boundary layer incorporating nanocrystals.

Special prominence has been paid to the investigation of the hybrid nanoliquid with energy and mass transmission. Because of its critical significance in engineering and innovation, it has attracted the attention of numerous scientists and experts [11–13]. Propagation of the hybrid nanoliquid flow, as well as energy transference, plays crucial roles in biotechnology, nuclear sectors, paper manufacturing, geophysics, chemical plants, and unusual lubricants are only some of the uses in industry [13–15]. Commonly used fluids cannot fulfill the global demands, in the era of scientific and technological advancement. However, comparable base liquids with the deposition of small particles showed a significant enhancement in thermal characteristics [16]. Currently, we have employed the Ag and MgO nanoparticles (NPs). The compound MgO is composed of the ions Mg^{2+} and O^2, which are joined by a special interaction. It is more useful for metalworking and electrical procedures. Similar to this, the antiseptic capabilities of Ag NPs could be used to change bioactivity in a diverse range of settings, including dental procedures, surgery, wound care, and pharmaceutical equipment [17]. A 3D numerical estimation of Ag–MgO-based nanofluid flow across a curved whirling disc, is investigated by Ahmadian *et al.* [18]. The hybrid composite was made by the addition of Ag–MgO NPs. By employing the numerical procedure parametric continuation method (PCM), the solution was found. Ag–MgO was considered to be more useful in addressing insufficient energy transport. Broad-spectrum antibacterial activities in metal and metal oxide nanomaterials have been extensively demonstrated for silver and MgO [19]. Anuar *et al.* [20] added MgO and Ag nanoparticulates, to produce a hybrid nanoliquid to evaluate boundary layer flow and temperature distribution. The consequences exposed that growing the weight fraction of Ag nanomaterials in a base fluid reduces the Nusselt number. Gangadhar *et al.* [21] have conducted a quantitative analysis of the properties of a nanofluid combining MgO and Au nanoparticles for convective heating. The influence of increased slip condition massively enhances the energy conduction ratio in the saddle and nodal point regions, according to the conclusions. Hiba *et al.* [22] inspected the thermal performance and fluidity of a water-based hybrid nanofluid made of MgO and Ag over a cylindrical, highly permeable region. Rasool *et al.* [15] examined numerical study of electromagnetohydrodynamic nanoliquid flows through a Riga pattern inserted diagonally in a Darcy–Forchheimer permeable media. Shah *et al.* [23] quantitatively investigated the convective fluxes of a remarkable non-homogeneous nanofluids mixture across an impenetrable longitudinal electrostatic substrate. Ashraf *et al.* [24] documented the nanoliquid flow using the generalized numerical approach.

The analysis of gyrotactic microbes in free surface flows has recently gained the attention of the scientific community. A microorganism is a living organism that can reproduce, evolve, react to environmental stimuli, and maintain a structured order. It can be utilized to improve oil recovery, which involves adding micronutrients and microorganisms to fuel layers to balance out permeability discrepancies [25–27]. The benefits of motile microbe interruption include nanofluid stability [28].

Hydrodynamic convection is created by oxytactic microbes, which forms a flow system that moves cells and oxygenation from the highest to the lowest fluid regions. The nanostructure mobility is regulated by molecular diffusion. The motile bacteria's motility seemed to be independent of nanomaterial gestures [29,30]. The working mechanism of gyrotactic microorganisms in nanofluid was first discussed in refs [29,31]. Kuznetsov [32] extended the idea of suspensions by including Buongiorno's conceptualization of bio-convection in nanoliquids. Xu *et al.* [33] analyzed a ferrofluid flow, consisting of motile microbes that flowed across parallel surfaces and transmitted energy. The velocity curve enhances with the mounting upshot of bioconvection [34]. Sohail *et al.* [35] examined the varied thermophysical characteristics of the 3D flow of a liquid with mass and energy conveyance in the presence of peristaltic transport of motile microbes over a curved elongated substrate. Despite the fact that the earlier analyses have indeed focused on understanding nanoliquid convection, there has been no effort in the literature to inspect the mass and motile microorganism transition under the influence of chemical reaction through the cylinder with sinusoidal radius (Figure 1).

The objective of this analysis is to scrutinize the features of the 3D stagnation point flow of Ag–MgO based hybrid nanoliquids traveling through a spherical cylinder with a harmonic radius. The electrostatic source consequences are evaluated in the stream flow. Our second priority is to elaborate also the uses and applications of silver and magnesium particles for medical and industrial

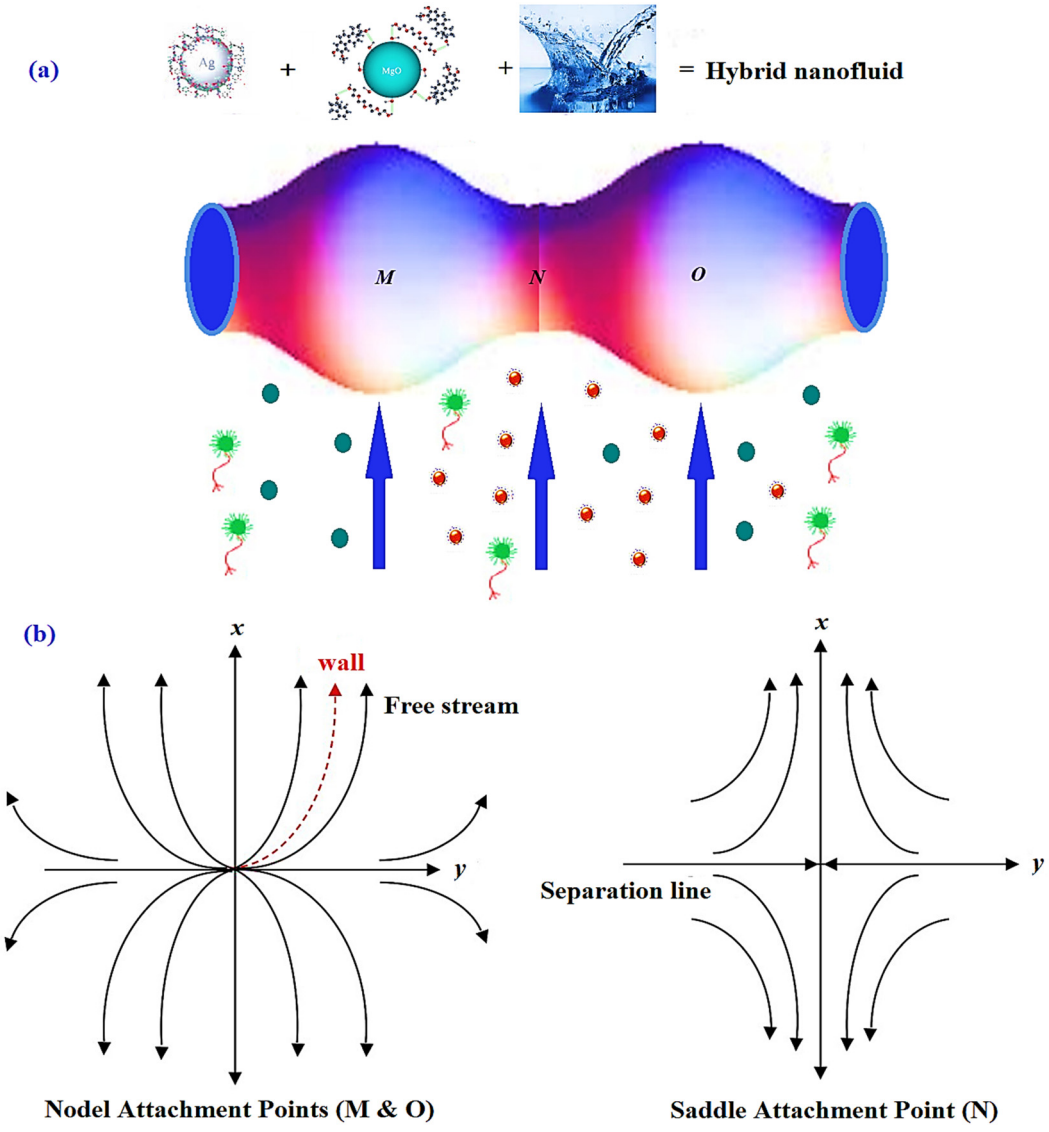

Figure 1: Physical configuration of the fluid flow.

purposes. After depersonalization, the computational technique PCM is used to calculate the powerful nonlinear systems. Furthermore, a pictorial assessment of the outstanding characteristics is performed on the velocity, mass, temperature, and motile microbes' profiles.

2 Mathematical formulation

We have presumed the 3D stream of Ag–MgO water-based hybrid nanofluids through a circular cylinder of the periodic surface. It is important to note that there exists a motionlessness point at each point M, N, and O. The u, v, and w are the velocities terms in the path of x, y, and z, respectively. Where

$$u_e^\star = xa^\star,\ v_e^\star = yb^\star.$$

Here, $a^\star$, $b^\star$are free stream coefficients. The streamlines are defined as $x_e^\star = \beta^{1/c}$, where β is constant and $c = b^\star/a^\star$. The nodal stagnation point appendix-lines span is $0 < c < 1$.

The flow pattern is shown in Figure 1(a). In Figure 1, point N is a saddle point, where points M and O are identified as nodal points. The streamlines in this respect are specified in Figure 1(b). Based on the above presumption, the basic equations can be described as [36,37]:

$$\frac{\partial u}{\partial r} + \frac{u}{r} + \frac{\partial w}{\partial z} = 0, \tag{1}$$

$$u\frac{\partial u}{\partial x} + v\frac{\partial u}{\partial y} + w\frac{\partial u}{\partial z} = xa^{\star 2} + \nu_{hnf}\frac{\partial^2 u}{\partial z^2}, \tag{2}$$

$$u\frac{\partial v}{\partial x} + v\frac{\partial v}{\partial y} + w\frac{\partial v}{\partial z} = yb^{\star 2} + \nu_{hnf}\frac{\partial^2 u}{\partial z^2}v, \tag{3}$$

$$(\rho C_p)_{hnf}\left(u\frac{\partial T}{\partial x} + v\frac{\partial T}{\partial y}\right) = k_{hnf}\frac{\partial^2 T}{\partial z^2}, \tag{4}$$

$$u\frac{\partial C}{\partial x} + v\frac{\partial C}{\partial y} = D_{hnf}\frac{\partial^2 C}{\partial z^2} - k(C - C_0), \tag{5}$$

$$u\frac{\partial N}{\partial x} + v\frac{\partial N}{\partial y} = D_n\frac{\partial^2 N}{\partial z^2}. \tag{6}$$

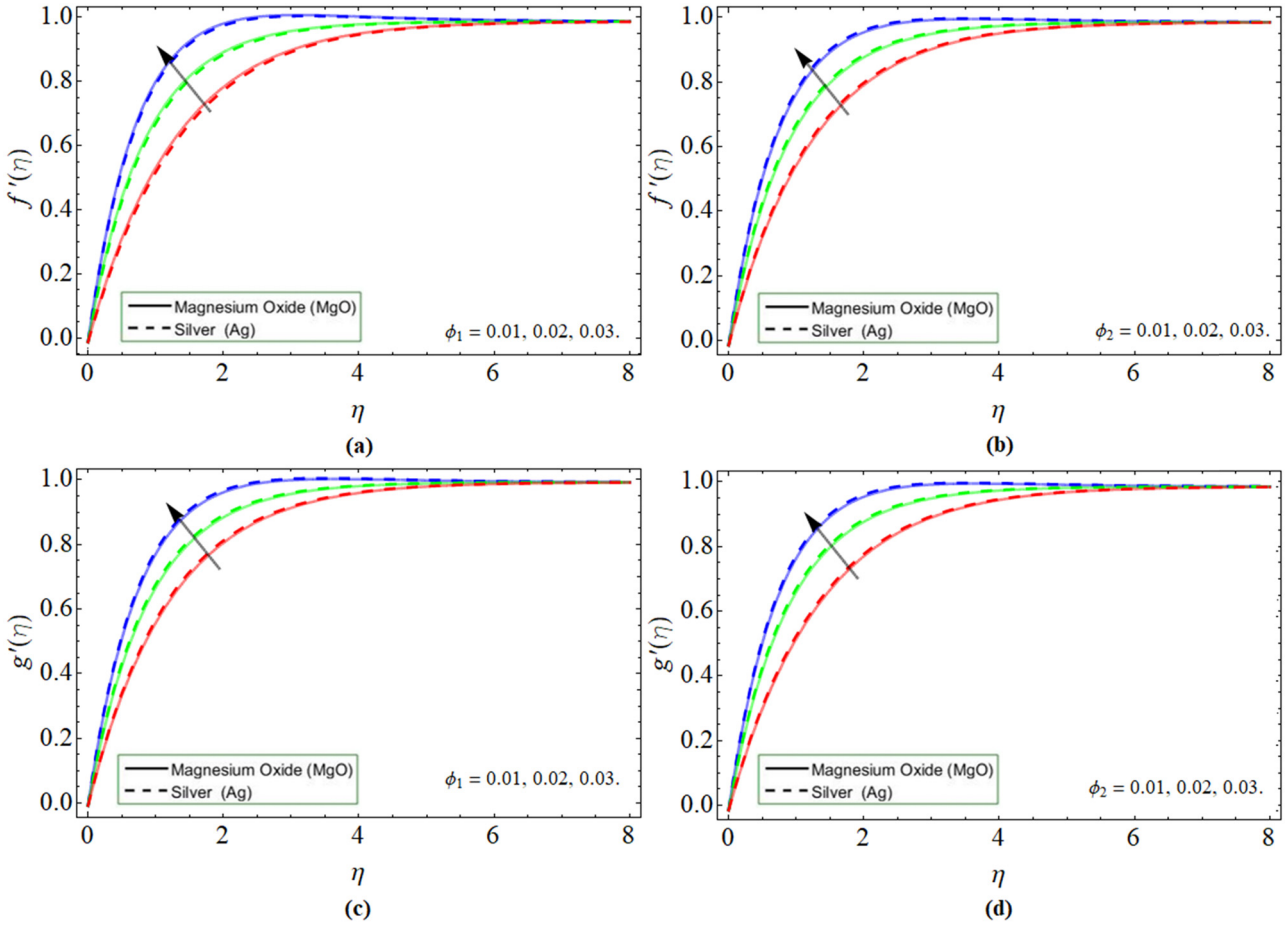

Figure 2: Exhibition of velocity ($f'(\eta)$, $g'(\eta)$) curve against volume fraction of silver ϕ_1 and magnesium oxide ϕ_2, while keeping $c = -0.5$ (dishes) and $c = 0.5$ (solid line).

Here, ν_{hnf}, D_{hnf}, and $(\rho C_p)_{hnf}$ are the kinematic viscosity, mass diffusivity, and volumetric heat capacity, where D_n is the microorganism diffusion and N is the motile microbe density.

The boundary conditions are:

$$\left.\begin{aligned} &u = 0,\ v = 0,\ w = 0,\ N = N_w,\ C = C_w,\\ &T = T_w \text{ at } z{=}0,\\ &u \to u_e^{\star},\ v \to v_e^{\star},\ T \to T_\infty,\ N \to N_\infty,\\ &C \to C_\infty \text{ when } z \to \infty. \end{aligned}\right\} \tag{7}$$

The thermophysical properties of hybrid nanoliquid and model are [9]:

$$\upsilon_{hnf} = \frac{\mu_{hnf}}{\rho_{hnf}}, \qquad \mu_{hnf} = \frac{\mu_f}{(1-\phi_{Ag})^{5/2}(1-\phi_{MgO})^{5/2}},$$

$$\frac{(\rho)_{hnf}}{(\rho)_f} = (1-\phi_{MgO})\left(1-\left(1-\frac{\rho_{Ag}}{\rho_f}\right)\phi_{Ag}\right) + \phi_{MgO}\left(\frac{\rho_{MgO}}{\rho_f}\right),$$

$$\frac{(\rho C_p)_{hnf}}{(\rho C_p)_f} = (1-\phi_{MgO})\left\{1-\left(1-\frac{(\rho C_p)_{Ag}}{(\rho C_p)_f}\right)\phi_A\right\} + \frac{(\rho C_p)_{MgO}}{(\rho C_p)_f}\phi_{MgO},$$

$$\frac{k_{hnf}}{k_{nf}} = \frac{k_{MgO} + 2k_{nf} - 2\phi_{MgO}(k_{nf} - k_{MgO})}{k_{MgO} + 2k_{nf} + \phi_{Cu}(k_{nf} - k_{MgO})},$$

$$\frac{k_{nf}}{k_f} = \frac{k_{Ag} + 2k_f - 2\phi_{Ag}(k_f - k_{Ag})}{k_{Ag} + 2k_f + \phi_{Ag}(k_f - k_{Ag})}.$$

In order to diminish the system of partial differential equations (PDEs) to the system of nonlinear ordinal differential equations (ODEs), we defined the following variables:

$$\left.\begin{aligned} &u = a^{\star}x\, f'(\eta),\ w = -\sqrt{a^{\star}\nu_f}\,(cg(\eta) + f(\eta)),\\ &v = b^{\star}y\, g'(\eta),\ \Theta(\eta) = \frac{T - T_\infty}{T_w - T_\infty},\\ &\Phi = \frac{C - C_\infty}{C_w - C_\infty},\ h = \frac{n - n_\infty}{n_w - n_\infty},\ \eta = z\sqrt{\frac{\nu_f}{a^{\star}}}. \end{aligned}\right\} \tag{8}$$

Now, by using Eq. (8) in Eqs. (1)–(6) and (7), we get:

$$A_1 f''' + cgf'' - f'^2 + ff'' + 1 = 0, \tag{9}$$

$$A_1 g''' + fg'' + cgg'' - cg'^2 + c = 0, \tag{10}$$

$$\frac{k_{hnf}}{k_f}\frac{1}{B_1\,\mathrm{Pr}}\Theta'' + f\Theta' + cg\Theta' = 0, \tag{11}$$

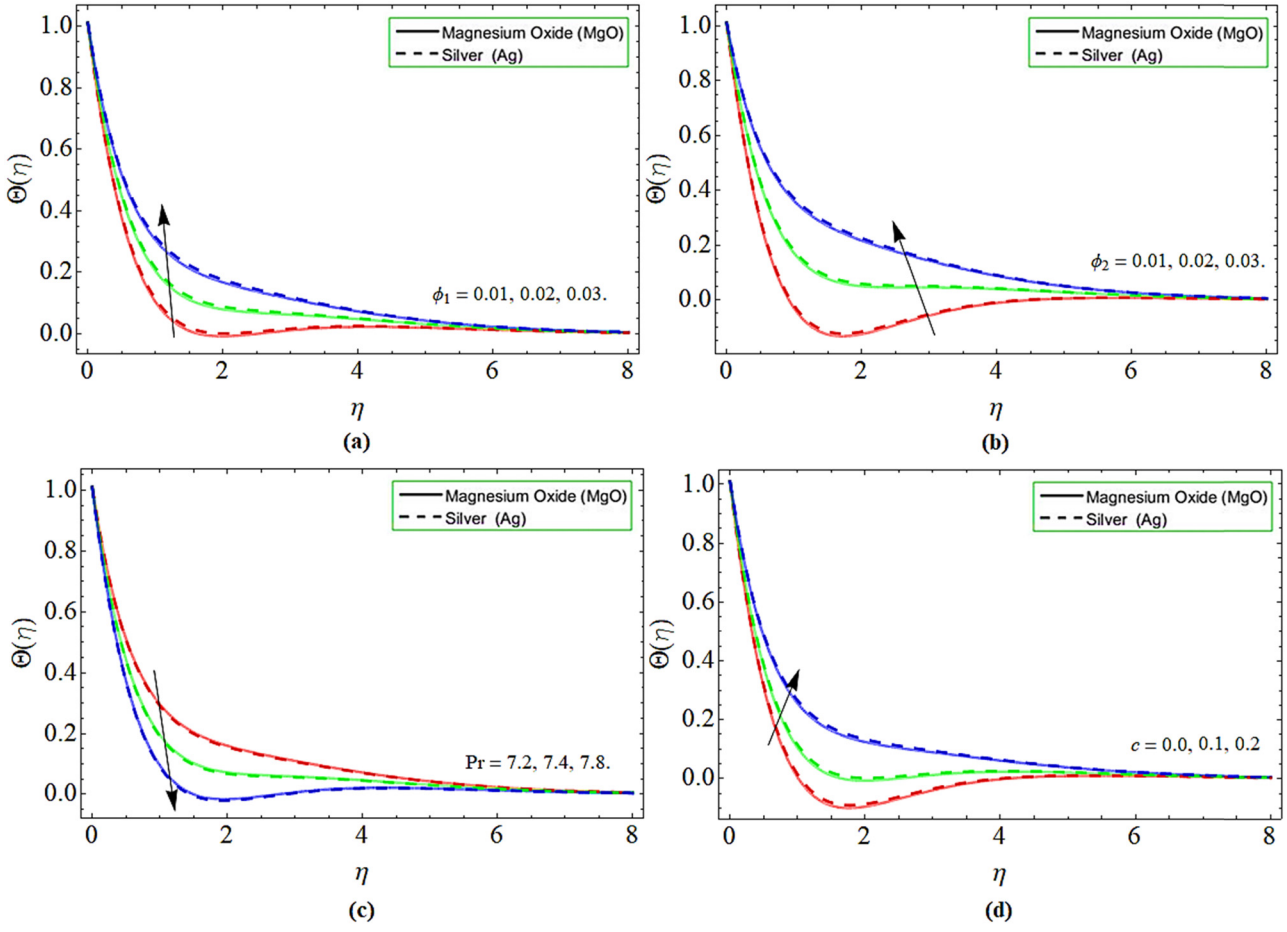

Figure 3: Exhibition of energy $\Theta(\eta)$ curve against (a) volume fraction of silver ϕ_1 (b) magnesium oxide ϕ_2 (c) Prandtl number (d) noddle point, while keeping $c = -0.5$ (dishes) and $c = 0.5$ (solid line).

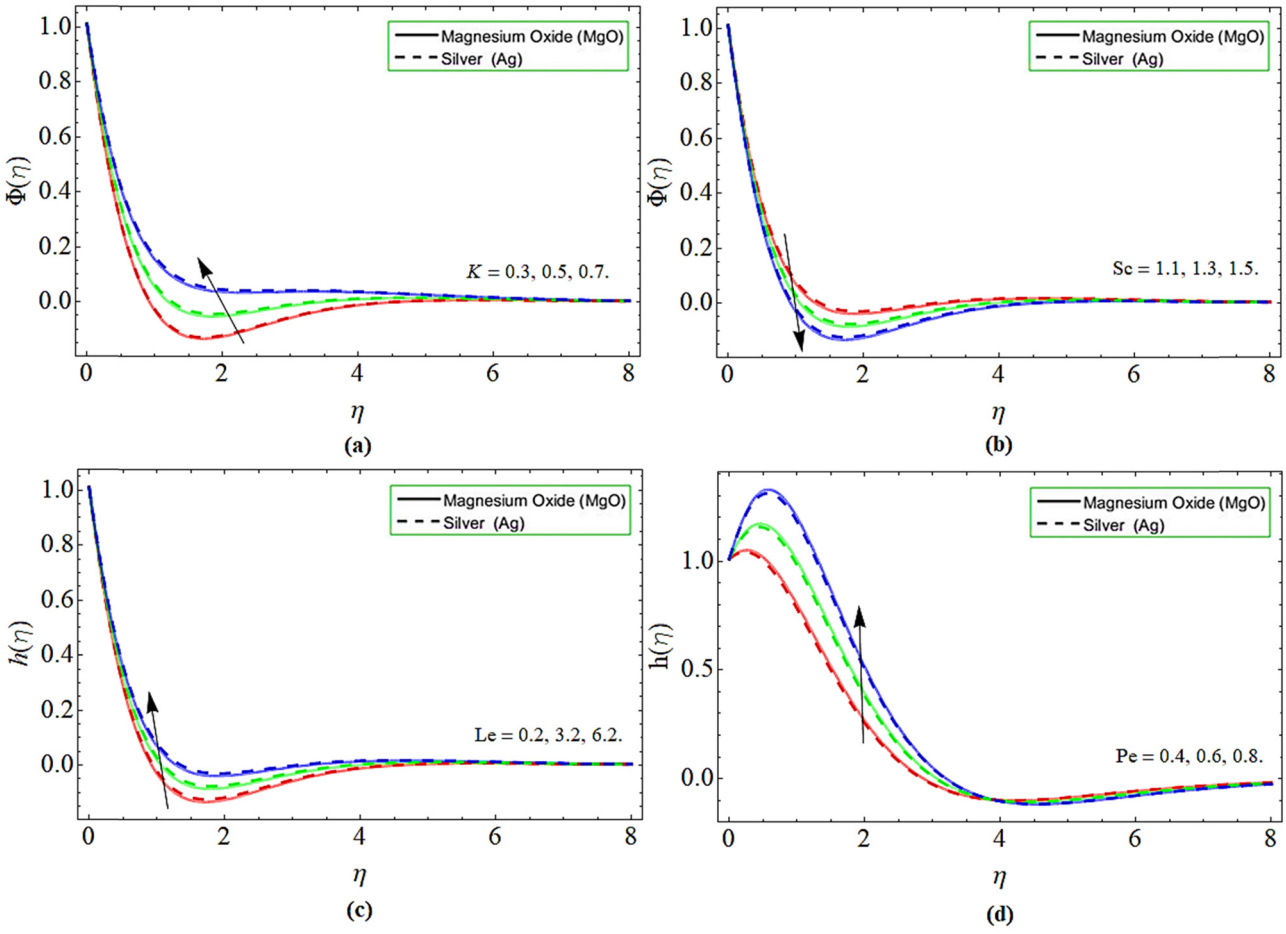

Figure 4: Behavior of mass transition $\Phi(\eta)$ and motile microbes $h(\eta)$ profile against (a) chemical reaction K, (b) Schmidth number Sc, (c) Lewis number, (d) Peclet number, while keeping $c = -0.5$ (dishes) and $c = 0.5$ (solid line).

$$\Phi'' C_1 - \mathrm{Sc}\,(f'\Phi') - K = 0, \tag{12}$$

$$h'' + (2\mathrm{Sc}fh' + (h'\Phi' - h\Phi'')\mathrm{Pe})\mathrm{Re} = 0. \tag{13}$$

Where,

$$A_1 = \left[(1-\phi_{\mathrm{Ag}})^{2.5}(1-\phi_{\mathrm{MgO}})^{2.5}\left(1-\phi_{\mathrm{MgO}}\left(1-\phi_{\mathrm{Ag}} + \phi_{\mathrm{Ag}}\frac{(\rho C_p)_{\mathrm{Ag}}}{(\rho C_p)_f}\right)\right) + \phi_{\mathrm{MgO}}\frac{(\rho C_p)_{\mathrm{MgO}}}{(\rho C_p)_f}\right],$$

$$B_1 = \left[\left(1-\phi_{\mathrm{MgO}}\left(1-\phi_{\mathrm{Ag}} + \phi_{\mathrm{Ag}}\frac{(\rho C_p)_{\mathrm{Ag}}}{(\rho C_p)_f}\right)\right) + \phi_{\mathrm{MgO}}\frac{(\rho C_p)_{\mathrm{MgO}}}{(\rho C_p)_f}\right], \tag{14}$$

$$C_1 = (1-\phi_{\mathrm{Ag}})^{2.5}(1-\phi_{\mathrm{MgO}})^{2.5}.$$

The renovated conditions are:

$$\left.\begin{aligned} &f'(0) = 0, f(0) = 0,\ g'(0) = 0,\ g(0) = 0,\\ &\Theta(0) = 1,\ \Phi(0) = 1,\ h(0) = 1 \text{ at } \eta = 0,\\ &f'(\infty) = 1, \Theta(\infty) = 0,\ g'(\infty) = 1,\ \Phi(\infty) = 0,\\ &h(\infty) = 0 \text{ as } \eta \to \infty. \end{aligned}\right\} \tag{15}$$

The physical interest quantities are:

$$C_{fx} = \frac{\tau_{wx}}{\rho_f U_w^2},\ C_{fy} = \frac{\tau_{wy}}{\rho_f U_w^2},\ Nu_x = \frac{xq_x}{k_f(T_w - T_\infty)}. \tag{16}$$

Where, τ_{wx}, τ_{wy}, and q_w are defined as:

Table 1: Experimental values of Ag, MgO, and water [9]

	ρ (kg/m^3)	C_p (J/kg K)	k (W/mK)	$\beta \times 10^5$ (K^{-1})
Pure water	997.1	4,179	0.613	21
Magnesium oxide	3,560	955	45	1.80
Silver	10,500	235	429	1.89

Table 2: Comparative assessment of PCM and bvp4c package for skin friction and the Nusselt number

	(ϕ_1, ϕ_2)	$\sqrt{Re_x}C_{fx}$		$x/y\sqrt{Re_x}C_{fy}$		$Nu_x\sqrt{Re_x}$	
		PCM	bvp4c	PCM	bvp4c	PCM	bvp4c
Ag	0.00	1.2683	1.2682	0.4994	0.4992	1.3304	1.3300
	0.01	1.9488	1.9385	0.7635	0.7629	1.6187	1.6183
	0.02	2.6974	2.6970	1.0621	1.0615	1.9296	1.9290
MgO	0.00	1.2686	1.2682	0.4999	0.4991	1.3321	1.3299
	0.01	1.6667	1.6659	0.6565	0.6556	1.4977	1.4954
	0.02	2.1541	2.1535	0.8482	0.8474	1.7396	1.7383

$$\tau_{wx} = \left((\mu_{hnf})\frac{\partial u}{\partial z}\right)_{z=0}, \quad q_w = \left(-(k_{hnf})\frac{\partial T}{\partial z}\right)_{z=0}, \quad \tau_{wy} = \left((\mu_{hnf})\frac{\partial v}{\partial z}\right)_{z=0}. \tag{17}$$

The dimensionless form of Eq. (16) is:

$$\sqrt{\mathrm{Re}_x C_{fx}} = \left(\frac{1}{(1-\phi_1)^{2.5}(1-\phi_2)^{2.5}}\right) f''(0),$$
$$(x/y)\sqrt{\mathrm{Re}_x C_{fy}} = \left(\frac{c}{(1-\phi_1)^{2.5}(1-\phi_2)^{2.5}}\right) g''(0), \tag{18}$$
$$\frac{Nu_x}{\sqrt{\mathrm{Re}_x}} = -\left(\frac{k_{hnf}}{k_f}\right)\theta'(0).$$

3 Problem solution

Different steps, which are used during applying PCM to system of Eqs. (9)–(13) and (15), are [38–43]:

Step 1: Reduced BVPs to the first order ODEs

$$\left.\begin{aligned} &f = \zeta_1,\ f'' = \zeta_3,\ g' = \zeta_5,\ \Theta = \zeta_7,\ \Phi = \zeta_9,\ h = \zeta_{11},\\ &f' = \zeta_2,\ g = \zeta_4,\ g'' = \zeta_6,\ \Theta' = \zeta_8,\ \Phi' = \zeta_{10},\\ &h = \zeta_{12}, \end{aligned}\right\} \tag{19}$$

By employing Eq. (19) to Eqs. (9)–(13) and (15), we get:

Table 4: Numerical outcomes of Nusselt number for the nanoliquid and hybrid nanoliquid

ϕ_{Ag}	ϕ_{MgO}	Ag–MgO/water	Ag/water	MgO/water
		$Nu_x\sqrt{Re_x}C_{fx}$	$Nu_x\sqrt{Re_x}C_{fx}$	$Nu_x\sqrt{Re_x}C_{fx}$
0.01	0.01	0.537	0.518	0.521
0.02	0.02	0.573	0.537	0.541
0.03	0.03	0.608	0.556	0.561
0.04	0.04	0.643	0.576	0.581

$$A_1\zeta'_3 + (cg + \zeta_1)\zeta_3 - \zeta_2^2 + 1 = 0, \tag{20}$$

$$A_1\zeta'_6 + (f + c\zeta_4)\zeta_6 - c\zeta_5^2 + c = 0, \tag{21}$$

$$\frac{k_{hnf}}{k_f}\frac{1}{B_1\,\mathrm{Pr}}\zeta'_8 + (f + cg)\zeta_8 = 0, \tag{22}$$

$$\zeta'_{10}C_1 - \mathrm{Sc}\,(f'\zeta_{10}) - K = 0, \tag{23}$$

$$\zeta'_{12} + \mathrm{Re}((2Sc\zeta_1 + \mathrm{Pe}\zeta_{10})\zeta_{12} - \mathrm{Pe}\zeta_{11}\zeta'_{10}) = 0. \tag{24}$$

boundary conditions are:

$$\left.\begin{aligned} &\zeta_1(0) = 0,\ \zeta_2(0) = 0, \zeta_4(0) = 0,\ \zeta_5(0) = 0,\\ &\zeta_7(0) = 1,\ \zeta_9(0) = 1,\ \zeta_{11}(0) = 1,\\ &\zeta_2(\infty) = 1, \zeta_5(\infty) = 1,\ \zeta_7(\infty) = 0,\ \zeta_9(\infty) = 0,\\ &\zeta_{11}(\infty) = 0. \end{aligned}\right\} \tag{25}$$

Table 3: Numerical outcomes of skin friction for the nano and hybrid nanoliquid

ϕ_{Ag}	ϕ_{MgO}	Ag–MgO/water		Ag/water		MgO/water	
		$\sqrt{Re_x}C_{fx}$	$x/y\sqrt{Re_x}C_{fy}$	$\sqrt{Re_x}C_{fx}$	$x/y\sqrt{Re_x}C_{fy}$	$\sqrt{Re_x}C_{fx}$	$x/y\sqrt{Re_x}C_{fy}$
0.01	0.01	1.300	0.450	1.231	0.423	1.231	0.424
0.02	0.02	1.451	0.513	1.300	0.450	1.303	0.453
0.03	0.03	1.647	0.591	1.380	0.482	1.388	0.485
0.04	0.04	1.882	0.687	1.471	0.518	1.482	0.523

Step 2: Familiarizing the embedding constraint p to Eqs. (20)–(24):

$$A_1\zeta'_3 + (cg + \zeta_1)(\zeta_3 - 1)p - \zeta_2{}^2 + 1 = 0, \quad (26)$$

$$A_1\zeta'_6 + (f + c\zeta_4)(\zeta_6 - 1)p - c\zeta_5{}^2 + c = 0, \quad (27)$$

$$\frac{k_{hnf}}{k_f}\frac{1}{B_1\,\mathrm{Pr}}\zeta'_8 + (f + cg)(\zeta_8 - 1)p = 0, \quad (28)$$

$$\zeta'_{10}C_1 - \mathrm{Sc}f'(\zeta_{10} - 1)p - K = 0, \quad (29)$$

$$\zeta'_{12} + \mathrm{Re}((2\mathrm{Sc}\zeta_1 + \mathrm{Pe}\zeta_{10})(\zeta_{12} - 1)p - \mathrm{Pe}\zeta_{11}\zeta'_{10}) = 0. \quad (30)$$

4 Results and discussion

The results are exposed through Figures (2–4), and Tables and discussion on the obtained results are categorized as:

4.1 Velocity profile

Figure 2(a)–(d) highlights the presentation of axial $f'(\eta)$ and radial velocity $g'(\eta)$ profile against volume fraction of silver ϕ_1 and magnesium oxide ϕ_2, while keeping c = −0.5 (dishes) and c = 0.5 (solid line), respectively. Both axial and radial velocities significantly enhance with the effect of hybrid nanoparticles (Ag–MgO). The heat absorbing capacity of water as compared to MgO and Ag nanomaterial is higher, so, adding more nanoparticles ($\phi_1 = \phi_2 = 0.01-0.04$) to water reduces its average heat capacity. That is why, such trend has been noticed.

4.2 Energy profile

Figure 3(a)–(d) uncovers the behavior of energy $\Theta(\eta)$ profile against the volume fraction of silver ϕ_1, magnesium oxide ϕ_2, Prandtl number, and noddle point, while keeping c = −0.5 (dishes) and c = 0.5 (solid line). Figure 3(a) and (b) manifest that the energy outline boosts with the increment of nanoparticulate in the base liquid. As we have discoursed before that the heat absorbing capacity of water as compared to MgO and Ag nanomaterial is higher, so adding more nanoparticles to water reduces its specific heat capacity. Figure 3(a) demonstrates that the energy distribution diminishes with the effect of Prandtl number. High effect Prandtl fluid has always low thermal diffusivity, so as a result of the current analysis, the Prandtl effect reduces the energy propagation rate. The energy transfer rate also improves at the noddle point as shown in Figure 3(d).

4.3 Mass and motile microorganism profile

Figure 4(a)–(d) emphasizes the performance of mass transition $\Phi(\eta)$ and motile microbes $h(\eta)$ profile against chemical reaction K, Schmidth number Sc, Lewis number, and Peclet number, while keeping c = −0.5 (dishes) and c = 0.5 (solid line). Figure 4(a) and (b) show that the upshot of chemical reaction enhances the mass transition because the chemical reaction parameter influence exercises the molecules inside the fluid, which encourages the mass transfer. On the other hand, the Schmidth number drops the mass transfer, because the kinetic viscosity of fluid augments with the action of the Schmidth number as reported in Figure 4(b). Figure 4(c) and (d) describes that the motile microorganism outline elevated with the increment of Lewis and Peclet number.

Table 1 presents the experimental values of Ag, MgO, and water. Table 2 discovers the comparative valuation of bvp4c package and PCM with the arithmetical outcomes of skin friction and the local Nusselt number. The variation of both Ag and MgO nanoparticles boosts the drag force and energy transference rate. From Table 2, it can be noticed that the PCM is fast approaching technique than bvp4c. Tables 3 and 4 report the comparison of simple and hybrid nanofluid behavior for skin fraction and energy transition. As compared to nanofluid, hybrid fluid has tremendous tendency for energy propagation.

5 Conclusion

We have observed the features of 3D stagnation point flow of Ag–MgO-based hybrid nanoliquids traveling through a spherical cylinder of sinusoidal radius. The facts have been formulated in the form of system of PDEs. After transformation, the computational technique PCM is used to estimate the nonlinear systems of differential equations. Furthermore, a graphical assessment of the physical characteristics is accomplished on the velocity, mass, temperature, and motile microbes' profiles. The key conclusions are as follows:

- Both axial and radial velocities significantly augment with the intensifying effect of hybrid nanoparticulates (Ag–MgO).
- The energy transmission profile also boosts with the increment of nanoparticulate in the base liquid.
- The energy transfer rate also improves at the noddle point.
- The upshot of chemical reaction enhances the mass transition because the chemical reaction parameter

influence exercises the molecules inside the fluid, whose encourages the mass transfer.
- The motile microorganism outlines elevated with the increment of Lewis and Peclet number.
- As compared to nanoliquid, hybrid nanoliquid is more convenient for heat and mass transmission.
- The skin friction coefficient augments with the rising numbers of nanoparticulates in the base fluid.
- The addition of MgO and Ag nanomaterials to the base fluid also enhances the Nusselt number.

Funding information: The author (Z. Raizah) extends her appreciation to the Deanship of Scientific Research at King Khalid University, Abha, Saudi Arabia, for funding this work through the Research Group Project under Grant Number (RGP.1/334/43).

Author contributions: All authors have accepted responsibility for the entire content of this manuscript and approved its submission.

Conflict of interest: The authors state no conflict of interest.

References

[1] Sohail M, Naz R. Modified heat and mass transmission models in the magnetohydrodynamic flow of Sutterby nanofluid in stretching cylinder. Phys A: Stat Mech Appl. 2020 Jul 1;549:124088.
[2] Wakif A. A novel numerical procedure for simulating steady MHD convective flows of radiative Casson fluids over a horizontal stretching sheet with irregular geometry under the combined influence of temperature-dependent viscosity and thermal conductivity. Math Probl Eng. 2020 May 5;2020.
[3] Wakif A, Chamkha A, Animasaun IL, Zaydan M, Waqas H, Sehaqui R. Novel physical insights into the thermodynamic irreversibilities within dissipative EMHD fluid flows past over a moving horizontal riga plate in the coexistence of wall suction and joule heating effects: a comprehensive numerical investigation. Arab J Sci Eng. 2020 Nov;45(11):9423–38.
[4] Cavanagh K, Wulandana R. 2D flow past a confined circular cylinder with sinusoidal ridges. In Proceedings of the 2019 COMSOL Conference in Boston. Boston, MA, USA; 2019 Oct. p. 2–4.
[5] Salahuddin T, Bashir AM, Khan M, Xia WF. Multiple shaped nano-particles influence on thermal conductivity of fluid flow between inflexible and sinusoidal walls. Case Stud Therm Eng. 2021 Jun 1;25:100930.
[6] Wu B, Li S, Zhang L, Li K. Experimental determination of the two-dimensional aerodynamic admittances of a 5: 1 rectangular cylinder in streamwise sinusoidal flows. J Wind Eng Ind Aerodyn. 2021 Mar 1;210:104525.
[7] Bilal M, Saeed A, Selim MM, Gul T, Ali I, Kumam P. Comparative numerical analysis of Maxwell's time-dependent thermo-diffusive flow through a stretching cylinder. Case Stud Therm Eng. 2021 Oct 1;27:101301.
[8] Seo YM, Luo K, Ha MY, Park YG. Direct numerical simulation and artificial neural network modeling of heat transfer characteristics on natural convection with a sinusoidal cylinder in a long rectangular enclosure. Int J Heat Mass Transf. 2020 May 1;152:119564.
[9] Bilal M, Khan I, Gul T, Tassaddiq A, Alghamdi W, Mukhtar S, et al. Darcy-forchheimer hybrid nano fluid flow with mixed convection past an inclined cylinder. Comput Mater Continua. 2021 Jan 1;66(2):2025–39.
[10] Alharbi KA, Ahmed AE, Ould Sidi M, Ahammad NA, Mohamed A, El-Shorbagy MA, et al. Computational valuation of darcy ternary-hybrid nanofluid flow across an extending cylinder with induction effects. Micromachines. 2022 Apr 9;13(4):588.
[11] Sohail M, Naz R, Abdelsalam SI. Application of non-Fourier double diffusions theories to the boundary-layer flow of a yield stress exhibiting fluid model. Phys A Stat Mech Appl. 2020 Jan 1;537:122753.
[12] Bilal S, Sohail M, Naz R. Heat transport in the convective Casson fluid flow with homogeneous–heterogeneous reactions in Darcy–Forchheimer medium. Multidiscip Model Mater Struct. 2019 Aug 16
[13] Algehyne EA, Wakif A, Rasool G, Saeed A, Ghouli Z. Significance of Darcy-Forchheimer and Lorentz forces on radiative alumina-water nanofluid flows over a slippery curved geometry under multiple convective constraints: a renovated Buongiorno's model with validated thermophysical correlations. Waves Random Complex Media. 2022 May 14;1–30.
[14] Bilal M, Gul T, Alsubie A, Ali I. Axisymmetric hybrid nanofluid flow with heat and mass transfer amongst the two gyrating plates. ZAMM-J Appl Math Mech/Zeitschrift für Angew Mathematik und Mechanik. 2021 Nov;101(11):e202000146.
[15] Rasool G, Shah NA, El-Zahar ER, Wakif A. Numerical investigation of EMHD nanofluid flows over a convectively heated riga pattern positioned horizontally in a Darcy-Forchheimer porous medium: application of passive control strategy and generalized transfer laws. Waves Random Complex Media. 2022 May 14;1–20.
[16] Tassaddiq A, Khan S, Bilal M, Gul T, Mukhtar S, Shah Z, et al. Heat and mass transfer together with hybrid nanofluid flow over a rotating disk. AIP Adv. 2020 May 1;10(5):055317.
[17] Li YX, Muhammad T, Bilal M, Khan MA, Ahmadian A, Pansera BA. Fractional simulation for Darcy-Forchheimer hybrid nanoliquid flow with partial slip over a spinning disk. Alex Eng J. 2021 Oct 1;60(5):4787–96.
[18] Ahmadian A, Bilal M, Khan MA, Asjad MI. Numerical analysis of thermal conductive hybrid nanofluid flow over the surface of a wavy spinning disk. Sci Rep. 2020 Nov 2;10(1):1–3.
[19] Zhang XH, Algehyne EA, Alshehri MG, Bilal M, Khan MA, Muhammad T. The parametric study of hybrid nanofluid flow with heat transition characteristics over a fluctuating spinning disk. PLoS One. 2021 Aug 16;16(8):e0254457.
[20] Anuar NS, Bachok N, Pop I. Influence of buoyancy force on Ag–MgO/water hybrid nanofluid flow in an inclined permeable

stretching/shrinking sheet. Int Commun Heat Mass Transf. 2021 Apr 1;123:105236.
[21] Gangadhar K, Edukondala Nayak R, Venkata Subba Rao M, Kannan T. Nodal/Saddle stagnation point slip flow of an aqueous convectional magnesium oxide–gold hybrid nanofluid with viscous dissipation. Arab J Sci Eng. 2021 Mar;46(3):2701–10.
[22] Hiba B, Redouane F, Jamshed W, Saleel CA, Devi SS, Prakash M, et al. A novel case study of thermal and streamline analysis in a grooved enclosure filled with (Ag–MgO/Water) hybrid nanofluid: Galerkin FEM. Case Stud Therm Eng. 2021 Dec 1;28:101372.
[23] Shah NA, Wakif A, El-Zahar ER, Ahmad S, Yook SJ. Numerical simulation of a thermally enhanced EMHD flow of a heterogeneous micropolar mixture comprising (60%)-ethylene glycol (EG),(40%)-water (W), and copper oxide nanomaterials (CuO). Case Stud Therm Eng. 2022 Apr 21;102046.
[24] Ashraf MU, Qasim M, Wakif A, Afridi MI, Animasaun IL. A generalized differential quadrature algorithm for simulating magnetohydrodynamic peristaltic flow of blood-based nanofluid containing magnetite nanoparticles: a physiological application. Numer Methods Partial Differ Equ. 2022 May;38(3):666–92.
[25] Hamad NH, Wakif A, Alshehri A. Towards the dynamics of a radiative-reactive magnetized viscoelastic nanofluid involving gyrotactic microorganisms and flowing over a vertical stretching sheet under multiple convective and stratification constraints. Waves Random Complex Media. 2022 Jul 20;1–31.
[26] Wakif A, Zaydan M, Alshomrani AS, Muhammad T, Sehaqui R. New insights into the dynamics of alumina-(60% ethylene glycol + 40% water) over an isothermal stretching sheet using a renovated Buongiorno's approach: A numerical GDQLLM analysis. Int Commun Heat Mass Transf. 2022 Apr 1;133:105937.
[27] Naz R, Tariq S, Sohail M, Shah Z. Investigation of entropy generation in stratified MHD Carreau nanofluid with gyrotactic microorganisms under Von Neumann similarity transformations. Eur Phys J Plus. 2020 Feb;135(2):1–22.
[28] Kuznetsov AV. The onset of nanofluid bioconvection in a suspension containing both nanoparticles and gyrotactic microorganisms. Int Commun Heat Mass Transf. 2010 Dec 1;37(10):1421–5.
[29] Geng P, Kuznetsov AV. Effect of small solid particles on the development of bioconvection plumes. Int Commun heat mass Transf. 2004 Jul 1;31(5):629–38.
[30] Naz R, Noor M, Shah Z, Sohail M, Kumam P, Thounthong P. Entropy generation optimization in MHD pseudoplastic fluid comprising motile microorganisms with stratification effect. Alex Eng J. 2020 Feb 1;59(1):485–96.
[31] Van Wijngaarden WK, Vermolen FJ, Van Meurs GA, Vuik C. Modelling biogrout: a new ground improvement method based on microbial-induced carbonate precipitation. Transp Porous Media. 2011 Mar;87(2):397–420.
[32] Kuznetsov AV. Non-oscillatory and oscillatory nanofluid bio-thermal convection in a horizontal layer of finite depth. Eur J Mechanics-B/Fluids. 2011 Mar 1;30(2):156–65.
[33] Xu YJ, Bilal M, Al-Mdallal Q, Khan MA, Muhammad T. Gyrotactic micro-organism flow of Maxwell nanofluid between two parallel plates. Sci Rep. 2021 Jul 26;11(1):1–3.
[34] Sohail M, Naz R, Abdelsalam SI. On the onset of entropy generation for a nanofluid with thermal radiation and gyrotactic microorganisms through 3D flows. Phys Scr. 2020 Feb 11;95(4):045206.
[35] Sohail M, Naz R, Shah Z, Kumam P, Thounthong P. Exploration of temperature dependent thermophysical characteristics of yield exhibiting non-Newtonian fluid flow under gyrotactic microorganisms. AIP Adv. 2019 Dec 1;9(12):125016.
[36] Gholinia M, Hosseinzadeh K, Ganji DD. Investigation of different base fluids suspend by CNTs hybrid nanoparticle over a vertical circular cylinder with sinusoidal radius. Case Stud Therm Eng. 2020 Oct 1;21:100666.
[37] Dinarvand S, Hosseini R, Damangir E, Pop I. Series solutions for steady three-dimensional stagnation point flow of a nanofluid past a circular cylinder with sinusoidal radius variation. Meccanica. 2013 Apr;48(3):643–52.
[38] Shuaib M, Bilal M, Qaisar S. Numerical study of hydrodynamic molecular nanoliquid flow with heat and mass transmission between two spinning parallel plates. Phys Scr. 2020 Nov 30;96(2):025201.
[39] Shuaib M, Shah RA, Bilal M. Variable thickness flow over a rotating disk under the influence of variable magnetic field: An application to parametric continuation method. Adv Mech Eng. 2020 Jun;12(6):1687814020936385.
[40] Shuaib M, Shah RA, Durrani I, Bilal M. Electrokinetic viscous rotating disk flow of Poisson-Nernst-Planck equation for ion transport. J Mol Liq. 2020 Sep 1;313:113412.
[41] Bilal M, Ayed H, Saeed A, Brahmia A, Gul T, Kumam P. The parametric computation of nonlinear convection magnetohydrodynamic nanofluid flow with internal heating across a fixed and spinning disk. Waves Random Complex Media. 2022 Mar 2;1–6.
[42] Algehyne EA, Areshi M, Saeed A, Bilal M, Kumam W, Kumam P. Numerical simulation of bioconvective Darcy Forchhemier nanofluid flow with energy transition over a permeable vertical plate. Sci Rep. 2022 Feb 25;12(1):1–2.
[43] Alrabaiah H, Bilal M, Khan MA, Muhammad T, Legas EY. Parametric estimation of gyrotactic microorganism hybrid nanofluid flow between the conical gap of spinning disk-cone apparatus. Sci Rep. 2022 Jan 7;12(1):1–4.